Vision-based Monitoring of the Short-term Dynamic Behaviour of Plants for Automated Phenotyping

Nikolaus Wagner
University of Lincoln
LN6 7TS Lincoln
United Kingdom
nwagner@lincoln.ac.uk

Grzegorz Cielniak
University of Lincoln
LN6 7TS Lincoln
United Kingdom
gcielniak@lincoln.ac.uk

Abstract

Modern computer vision technology plays an increasingly important role in agriculture. Automated monitoring of plants for example is an essential task in several applications, such as high-throughput phenotyping or plant health monitoring. Under external influences like wind, plants typically exhibit dynamic behaviours which reveal important characteristics of their structure and condition. These behaviours, however, are typically not considered by state-of-the-art automated phenotyping methods which mostly observe static plant properties. In this paper, we propose an automated system for monitoring oscillatory plant movement from video sequences. We employ harmonic inversion for the purpose of efficiently and accurately estimating the eigenfrequency and damping parameters of individual plant parts. The achieved accuracy is compared against values obtained by performing the Discrete Fourier Transform (DFT), which we use as a baseline. We demonstrate the applicability of this approach on different plants and plant parts, like wheat ears, hanging vines, as well as stems and stalks, which exhibit a range of oscillatory motions. By utilising harmonic inversion, we are able to consistently obtain more accurate values for the eigenfrequencies compared to those obtained by DFT. We are furthermore able to directly estimate values for the damping coefficient, achieving a similar accuracy as via DFT-based methods, but without the additional computational effort required for the latter. With the approach presented in this paper, it is possible to obtain estimates of mechanical plant characteristics in an automated manner, enabling novel automated acquisition of novel traits for phenotyping.

1. Introduction

In modern agricultural applications, computer vision and its potential for automating many laborious tasks play an increasingly important role. Phenotyping, monitoring plant health and even selective harvesting [28] are all tasks that can benefit from the capabilities of modern technology in order to reduce the necessary amount of human labour. To this end, an automated system surveying the state of plants with the help of state-of-the-art (SOTA) computer vision tools is crucial for enabling the automation potential of all of these applications. The majority of current research in this domain focuses on monitoring static plant properties such as shape, colour, complexity or structure [10]. Plants however are highly dynamic and motile systems, often experiencing motion caused by external forces such as wind [22] or physical interactions, like the ones necessary in crop picking applications [27]. The short-term dynamic responses of plants to these interactions are often characterised by oscillatory motions which are an indicator of internal plant properties. These properties may include their rigidity and ability to withstand strong wind or heavy rain,

Figure 1: The oscillatory movement of a wheat ear after excitation in an image sequence together with the trace of a marker and an estimate of f [Hz] and β [s^{-1}] at four progressive points in time.

but also their more acute health status, including for example water stress [5]. Due to that, an increasing amount of scientific consideration has been given to the dynamic mechanical properties of plants for computer vision-based agricultural applications in the recent past.

In this paper, we propose an automated monitoring system for estimating key dynamic plant properties from video data acquired via a standard RGB camera. In our system, we use colour-based markers to localise and track individual plant parts undergoing dynamic oscillatory motion, like fluttering, waving or shaking. We subsequently use the velocity of the tracked marker as input data for spectral analyses, estimating the eigenfrequency and damping coefficient of the observed motion. The velocity of the marker is used instead of the raw position since velocity is phase-shifted but directly correlated to the position, which therefore eliminates any static bias while still accurately representing the dynamic changes. We rely on artificial markers for motion tracking and focus our investigations in this paper on the deduction of dynamic plant properties, not dealing in close detail with the intricate technicalities of marker detection and motion tracking. It has however been shown previously that it is also possible to derive oscillatory plant motions directly from video data using optical flow instead of dedicated markers [26], which provides the potential for a fully automated pipeline.

In summary, this paper introduces the following key contributions:

- an approach for estimating the frequency f and the damping coefficient β of plants from video sequences with the help of harmonic inversion;
- identification of the critical parameters of the method, their respective influences on the results and comparison against classical spectral analysis methods based on Fourier transform;
- an evaluation of the performance of our method in real-life scenarios with various moving plants exhibiting several characteristics and under different data acquisition regimes.

2. Related Work

The automation potential of high-throughput phenotyping and the possible use of computer vision for it has been a highly active area of research in recent years. This has been highlighted recently on the example of strawberry plants in a comparative study by James et al. [10]. The key characteristics used for phenotyping are typically of a static nature, like length or general size of individual plant parts, or simply colour and location of fruit [19]. Some temporal traits have been considered in the past, like growth rate [14] and flowering duration [8]. More recently, however, the short-term dynamics, characterising movement on the scale of seconds rather than days or weeks, has started to gain attention for these purposes as well.

Some recent work underlines the potential importance of the dynamic properties of plants, specifically oscillatory movements, for phenotyping and other agricultural applications. For example, Jung et al. have recently demonstrated the significance of the fluttering dynamics of leaves, which can be a valuable indicator of the water stress level of plants [13] and give useful insights into a plant's fitness for a certain climate. Leaf flapping dynamics are investigated in more detail in recent work by Bhosale et al. in which the authors study the reaction of leaves to the impact of raindrops [2]. Even further analyses of leaf flutter are given in [25], highlighting its important contribution to the resilience of trees to wind damage.

In [3], Brüchert et al. give a detailed mechanical description of plants that are "top loading with negligible stem mass", like wheat ears for example, illustrating the correlation between the oscillation frequency of plants, the dimensions and weight of their parts as well as their elasticity. Similarly, de Langre et al. have recently studied plant vibrations at all scales [5] and even provide a specific investigation of utilising free plant oscillations to phenotype poplar (*Populus sp.*), tobacco (*Nicotiana benthamian*) and wheat (*Triticum aestivum L.*) plants [6] with respect to parameters like changes in mass and the internal levels of water stress that the plant experiences. Both of these attributes are highly relevant for phenotyping in order to breed plants which are well suited for hotter climates and more resilient to buckling. Furthermore, this work also relates closely to previous investigations by Nakata et al. [20], who utilise stem vibrations to identify mutants of thale cress (*Arabidopsis thaliana*), highlighting again the usefulness of oscillatory parameters for phenotyping purposes.

All these examples focus mostly on undamped oscillations, however damping plays an important role in naturally oscillating plants as well, mostly for the purpose of protecting the structural integrity of the plant by distributing energy efficiently among its entire structure or into the surrounding media [9][22]. These different modes of damping and their effects are thus very relevant for phenotyping purposes as well, since they help to select more resilient and robust plants. The respective effects have been studied intensely for example in work by Castro-Garcia et al. [4] who investigate the different modes of oscillation and their individual damping behaviours. Spatz et al. have investigated the contribution of different types of branches to oscillation damping in trees [23], while Jonsson et al. have documented the effects, be they structural or caused by the surrounding media, that lead to the actual phenomenon of damping in plants [12]. It is therefore obvious that damping

in plants is just as important an area of investigation as the phenomenon of plant oscillations itself.

All this highlights the possibility of, as well as the demand for, using short-term dynamics and oscillatory motion in modern phenotyping and automated plant monitoring applications. Simultaneously, it also underlines the difficulties and possible downsides of this approach, with the time needed to actually perform measurements and the tools used to collect and evaluate data being some of the biggest hindrances. Therefore, by improving this process and automating as much of it as possible, large benefits can be brought to the area of high-throughput phenotyping and autonomous crop monitoring.

The tools needed for enabling us to collect these data efficiently are therefore twofold. On the one hand, we require standard SOTA computer vision tools for detection and tracking, which are typically available as off-the-shelf solutions [1][26]. On the other hand, we need a toolset to determine the oscillatory parameters themselves. For analysing spectral behaviours in general, Fourier transform has been the default choice in the recent past, specifically discrete Fourier transform (DFT) is most commonly used [24]. Nevertheless, while DFT is a well-established, straightforward method for spectral analyses, its capabilities in terms of dealing with decaying signals, i.e. damped oscillations like the movement of wheat ears as illustrated above, are limited. It is therefore relevant to also consider other approaches, like harmonic inversion (HI) [18]. HI takes the approach of dividing the input signal into a combination of decaying sine waves. By doing so, it provides an insight not only into which frequencies are the most dominant in the input signal but also into their decay rate / damping ratio, which as highlighted previously can be a valuable indicator for various plant health-related factors and more.

3. Dynamic Plant Behaviour Monitoring

In this section, we describe the process we employ in order to determine the short-term dynamic parameters of plants in more detail. We start off by applying colour-based tracking markers on different types of plants and plant organs. We then detect and track these markers using simple colour-based thresholding and a standard object tracking algorithm (i.e., SORT [1]) to obtain their movement data (as for example shown in Fig. 1). We use these data to obtain reference values for ground truth (GT) data of their dynamic oscillation behaviour, however in a fully automated system, as for example presented by Wagner & Cielniak [26], no markers are necessary to obtain these values, which allows for a high degree of automation.

Subsequently, we excite the plant parts manually and use the velocity of the tracked markers (in the image pixel domain), sampled at a camera frame rate of $f_s = 200$ Hz over a period of 10 s after excitation. This manual act of excitation

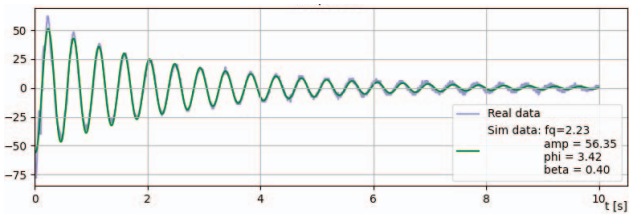

Figure 2: Ringdown behaviour of a wheat ear (see also Fig. 1 for reference), illustrated as the velocity (in pixels) of a tracked marker over time. Data calculated using a fitting oscillator model are shown for reference as well.

can be easily automated for example by an articulated robot arm to increase the degree of automation of this method. For the purpose of our experiments however this did not prove to be necessary and we therefore leave it for future work or in-field applications.

As mentioned above, the data annotation we utilise is performed in image-pixel space. Since we are not particularly interested in the absolute magnitude of movement at this point but primarily in frequency and damping parameters, we assume that a transformation to real-world coordinates or even 3D space is not necessary. Both of the observed quantities are scale-invariant, therefore this assumption holds. An example of the input data thus obtained is illustrated in Fig. 2.

The behaviour observed in this figure, commonly known as “ringdown”, can be modelled by the well-known equation for the classical damped harmonic oscillator, defined by Eq. (1) as

$$x_{(t)} = x_0 \cdot e^{-i(2\pi f t - \phi) - \beta t}, \tag{1}$$

wherein x_t is the amplitude at a given point in time t with x_0 being the initial amplitude at $t = 0$, f is the frequency, ϕ the phase and β the decay rate, representing the damping of the system. From all the parameters introduced by this equation, for our purposes we are particularly interested in f and β, as they enable us to obtain a deeper understanding of the state and behaviour of a plant. Nevertheless, we implicitly also obtain measures of ϕ and x_0 as well. These parameters hold the potential for further evaluation in future work, however for the purposes of this paper we do not consider any significance they may hold and focus on f and β instead. To actually obtain numerical values for these parameters, we require spectral analysis methods, which we now discuss in the following section.

4. Spectral Analysis Methods

Analysing the spectral components of signals is a well-established area of research, as they hold great significance for many applications in e. g. electrical or mechanical engi-

neering. As such, several approaches to this problem exist. While the most popular choice for extracting the spectral components of a signal is arguably DFT, HI provides various advantages over the classical Fourier-based analyses. Specifically, HI holds the potential for a much higher frequency resolution and grants insight into the damping behaviour of signals directly without the need for additional computation. In this section, we investigate both methods and highlight their respective peculiarities and strengths.

4.1. Harmonic Inversion

The harmonic inversion of time signals is an approach to spectral analysis which fundamentally operates on the assumption that the investigated signal is constituted of a number of decaying oscillations with different parameters and attempts to find the determining parameters of these.

The problem can be formulated as a non-linear fit of a signal C sampled at τ equidistantly spaced points:

$$C_{(n\tau)} = \sum_{k=1}^{K} d_k e^{-in\tau\omega_k}, \qquad n = 0, 1, 2, ..., N \tag{2}$$

Eq. (2) introduces K sets of parameters, with d_k describing the amplitude and the real part of ω_k the frequency of a certain signal component. HI imposes no restrictions on the closeness of these components, allowing in theory for an arbitrarily high resolution of the results, depending on the results of the non-linear fit. Furthermore, by also using the imaginary part of ω_k the width of the frequencies can be deduced, thus their decay rates can be calculated directly.

To solve the nonlinear set of equations from Eq. (2), at least $N = 2K$ points are required, with the method being most efficient and stable with K no larger than 50 - 200 [15]. Choosing an appropriate value for K, the number of frequencies to be identified, is thus essential for the performance of the algorithm. In practice it is also essential to define a frequency range for the algorithm, with plants typically exhibiting oscillations in the range from 0.5 - 10Hz.

The mathematical intricacies of the harmonic inversion problem are complex and exceed the scope of this paper. We refer the interested reader to the explanations presented in [18], [16] & [17], and for implementation details to [11].

4.2. Fourier Transform

A standard approach to spectral analysis, the mathematical definition of the Fourier transform for a discrete time series of complex numbers $x_0, ..., x_{N-1}$ is given as

$$X_{(k)} = \sum_{n=0}^{N-1} x_n e^{\frac{-i2\pi kn}{N}} \tag{3}$$

wherein $X_{(k)}$ represents the magnitude of a frequency component k present in the input series x with $k = 0, 1, 2, ..., N-1$. DFT thus basically iterates over a finite number of frequency components and provides information about the presence of each of these frequency components in the signal.

The main difference in this equation in comparison to the definition of HI is that while in HI the frequency components can be arbitrarily close, DFT imposes a restriction on the granularity of the calculated frequency "bins", with them being all equally sized. Furthermore, the resolution in the frequency domain for DFT is not only determined by the sampling rate f_s but also by the number of samples N, so that the frequency resolution Δf, i.e. the size of one bin, is defined as per Eq. (4) as

$$\Delta f = \frac{f_s}{N} = \frac{1}{T} \tag{4}$$

for a data collection period of length T. The range of frequencies that can be observed is in theory mathematically limited to a maximum of $N \cdot \Delta f = f_s$. However, in accordance with the Shannon-Nyquist sampling theorem, only frequencies of up to $\frac{f_s}{2}$ can be accurately described [21].

Finally, DFT can not directly provide information about the decay value of a signal since it only provides insights into frequency components in a signal for one point in time. To obtain information about signal decay, additional steps are necessary, as will be illustrated in Section 5.2.

For the calculation of all DFTs in this paper, we have utilised the implementation as a fast Fourier transform (FFT) from the numpy library [7], we are therefore using DFT and FFT interchangeably hereinafter.

5. Implementation Details

5.1. Harmonic Inversion

For harmonic inversion, we initially have to define a range of frequencies to search in, as well as a number of signal components K to reconstruct the input signal from, as explained in Section 4.1. The frequency range needs to be restricted relatively closely around the frequency of interest since HI tends to otherwise also pick up the harmonics of the actual eigenfrequency. In our investigations, we therefore limit the frequency range to roughly $\pm 90\%$ around the frequency of interest, to block the influence of any harmonics. In practice, most oscillatory motions in plants occur below 10 Hz. The correct value for K needs to be selected carefully as well since too small values produce less accurate results and too large values lead to inefficient calculations and thus require increased processing time. In practice, a value of $K = 200$ as recommended in [15] has proven to work well, which is why all further analyses in this paper use $K = 200$, unless otherwise specified.

From performing the harmonic inversion of the input signal, we obtain a series of signal components, each charac-

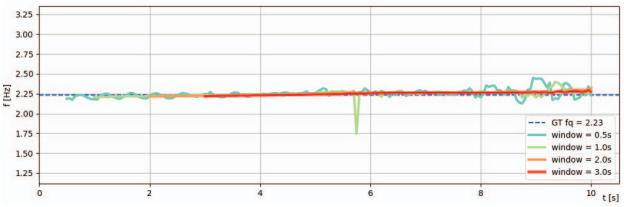

Figure 3: Frequency values calculated using HI on data obtained from Scenario 1 with a moving window of varying length.

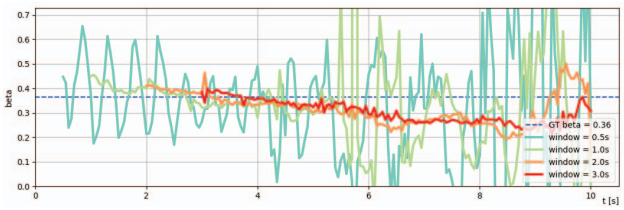

Figure 4: Decay values obtained directly by running HI on data obtained from Scenario 1 with a moving window of varying length.

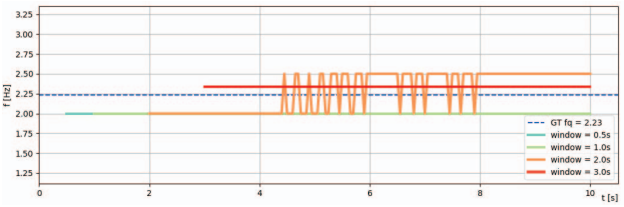

Figure 5: Frequency values calculated using FFT on data obtained from Scenario 1 with a moving window of varying length.

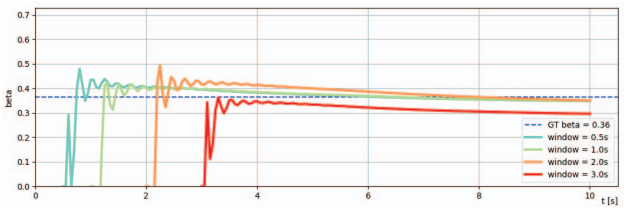

Figure 6: Decay values calculated from a curve fit on the amplitudes obtained by running FFT on data obtained from Scenario 1 with a moving window of varying length.

terised by f, x_0, ϕ, β and a subjective error value that describes the methods' "confidence" in a specific component. To further de-noise the results, we disregard components with negative values for the damping coefficient β (i. e. signals growing in magnitude) and components which are overdamped (i. e. components where $\beta > 2\pi f$, which would allow for no oscillation at all). From the remaining components, we select the one with the lowest error value and use those values for f and β. By doing so, we are able to obtain much more accurate results for f than the ones obtained with FFT, as can be seen in Fig. 3 and Fig. 5. We also directly obtain values for β, which are correspondingly shown in Fig. 4, however, the improvement in accuracy of these values in comparison to the ones produced by FFT (as shown in Fig. 6) is less obvious and highly dependent on the amount of input data available.

5.2. Fourier Transform

Using FFT, it is a straightforward matter to obtain the dominant frequency from a signal such as the one shown in Fig. 2. We perform the actual FFT on the same input data as for HI, crop the obtained spectral signature to a frequency range of interest to reduce the possible impact of noise and select the bin with the highest magnitude. If we run this algorithm continuously for a moving window of length T over the input data, the calculated frequency result will develop as shown in Fig. 5.

The accuracy of the results depends strongly on the amount of data available, i. e. the value of T. For example, in accordance with Eq. (4), the smallest granularity we can achieve for $T = 3.0\,\mathrm{s}$, the largest T used in this experiment, is $\Delta f = 0.33\,\mathrm{Hz}$. For frequencies in our comparatively low range of interest, this is significant, leading to an uncertainty range of roughly 15 % for $f = 2.2\,\mathrm{Hz}$.

Also, obtaining a decay value is not directly possible by using FFT. To address this issue, we utilise the signal amplitude values which can be directly obtained from FFT, store them and perform a curve fit on all available amplitudes. As the model for this fit, we can use the decay function from Eq. (1) with $f = 0$ and $\phi = 0$, which leaves only x_0 and β as unknowns. Since we can use $x_{(0)}$ as x_0, we only need to obtain a value for β, which can be obtained through a least-square-fit. By doing so, we get a gradually refining value for β, as shown in Fig. 6 which also highlights the differences stemming from the use of different window lengths on the results, with a more thorough evaluation presented in the following sections.

To further evaluate both of the introduced approaches and compare them appropriately, we now perform numerical comparisons in Section 6.

6. Evaluation

6.1. Methodology

To test the suitability of our approach for obtaining oscillation parameters from plant motion, we first define GT data to compare our results against. For this, we manually select fitting values for the parameters of Eq. (1) in order to represent the movement data shown in Fig. 2 accurately. We then fine-tune these parameters with the help of a least-square fit

T		0.5 s	1.0 s	2.0 s	3.0 s	IW
HI	f	1.0 %	0.9 %	0.6 %	0.6 %	0.4 %
	β	34.9 %	43.6 %	11.7 %	11.1 %	5.2 %
FFT	f	10.4 %	10.4 %	10.9 %	4.5 %	3.1 %
	β	7.3 %	6.2 %	11.2 %	9.5 %	61.2 %

Table 1: Mean percentage error for frequency and decay calculated using HI or FFT with different evaluation window sizes as well as an increasing-size window.

to ensure the most accurate representation possible. The oscillation behaviour thus defined by these parameters is plotted in Fig. 2 and aligns closely with the GT data as well, which underlines the validity of the oscillator model. From this, we can also observe the good correspondence of the calculated GT data to the real data collected from the video sequences. The parameters obtained in this way are therefore used as reference values for our further evaluations. As mentioned above however, we do not address the issue of tracking plant parts and assume marker-provided, perfect data. In practice, this component is a possible source of additional error introduced into the system.

To evaluate the performance of the different spectral analysis methods, we infer f and β from the oscillation data obtained from the video sequences, as shown in Fig. 1, using both methods. We then compare the determined parameters against our GT data. By doing so, we obtain an estimate of the accuracy and performance of HI in comparison to FFT. For evaluation purposes, we subsample the input data with a moving fixed-size window of different lengths T as well as an increasing-size window and investigate the influence of these two sampling methods on the results.

6.2. Critical Parameters

In the first step, we evaluate the influence of the type and size of the evaluation window used on the results of the analyses. We use fixed-size windows with a length of T = 0.5 s, 1.0 s, 2.0 s and 3.0 s as well as a window of increasing length which continuously accumulates data. As input data, we use the plant movement data shown in Fig. 2.

To evaluate the performance of HI vs. FFT, we define a "stable period" in which we analyse the results by comparing them to the manually defined GT values as explained in Section 3. For the increasing-size window, this stable period starts as soon as 2 K samples are available as this is the minimum required for HI to be able to solve the nonlinear fit as explained in Section 4.1. For a fixed-size, moving evaluation window, the stable period starts after 1.5 T. In both cases, the stable period ends when the oscillation amplitude becomes less than 10 % of its original magnitude. By utilising this period we attempt to suppress the influence of noise and low-confidence calculations. All metrics in this section

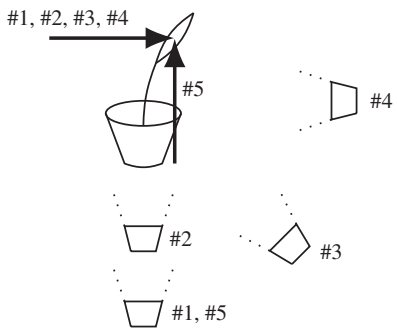

Figure 7: Camera positions and excitation modes used in the different evaluation scenarios for a wheat ear.

evaluate the data inside this period. We now calculate f and β using the various fixed-size windows and compare them to the GT values inside the stable period. The respective mean error values are given in Table 1.

From this initial investigation, we can observe that a larger window consistently leads to better results for f. For β however, the influence of T is less linear. When using HI, a larger T almost universally leads to better results for β as well (except for $T < 2.0$ s, since at $f_s = 200$ Hz a smaller value for K is required than for the other window sizes, as explained in Section 4.1, which leads to less predictable results). Conversely, the FFT based calculations for β utilise the average signal amplitude in the evaluation window for the curve fit, therefore an increased window size artificially flattens the decay of the curve, thereby worsening the obtained estimates of β.

In practice, therefore, we choose an increasing-size window for all evaluation scenarios except for the calculation of decay by FFT, for which we choose T = 1.0 s. As shown in Table 1, these values produce the best results for the respective tools and thus allow for a fair comparison.

6.3. Evaluation Scenarios

We perform several experiments with an increasing-size window as well as with a fixed-size window of T = 1.0 s in different scenarios. In the first step, we record diverse data of an oscillating wheat ear such as illustrated in Fig. 2, which exhibited an eigenfrequency of $f = 2.2$ Hz and a decay value of $\beta = 0.4$ along its main axis of oscillation. The 5 different data recording scenarios we used in this analysis, in which we varied camera position as well as direction of excitation, are illustrated in Fig. 7. Scenario 1 is equivalent to the one used for primary analyses in the previous section and will thus serve as a point of reference.

As above, we calculate the mean percentage error for f and β for each scenario. The results, using an increasing-size window for all calculations except for the calculation of β by FFT as explained above, are given in Table 2.

Scenario		#1	#2	#3	#4	#5
HI	f	0.4 %	0.3 %	0.4 %	0.3 %	2.5 %
	β	10.5 %	4.7 %	7.6 %	8.5 %	44.3 %
FFT	f	3.1 %	3.1 %	3.1 %	3.2 %	5.6 %
	β	6.2 %	7.9 %	6.6 %	2.4 %	37.8 %

Table 2: Mean percentage error for frequency and decay estimates of wheat ears calculated using HI and FFT respectively. A fixed-size, moving evaluation window (T = 1.0 s) was used for the calculation of β by FFT and an increasing-size window was used for all other calculations.

Scenario	#1 - 5	#6	#7	#8	#9	#10
f [Hz]	2.23	0.63	1.76	1.62	1.97	1.53
β [s^{-1}]	0.40	0.11	0.95	0.72	0.61	0.79

Table 3: Ground truth values for f and β of the different plants / plant parts illustrated in Fig. 1 & Fig. 9.

It is immediately apparent that the worst results are obtained when changing the direction of excitation. This is because the direction of excitation for Scenarios 1 - 4 is in the plane of oscillation of the wheat ear, while the direction of excitation in Scenario 5 is perpendicular to it. Because of this, the wheat ear changes direction mid-oscillation to return to its main oscillation axis, experiencing a phase-shift as well as losing some oscillation energy, both of which influence the analyses negatively.

We can also see that in all other cases, the results for f obtained by HI are not only roughly ten times more accurate than the results obtained by FFT, but also below 1% mean percentage error. The calculated values for β are in most cases marginally better when calculated by FFT, however the differences are not very large and HI is able to provide these values directly without any additional computation steps, unlike FFT. To illustrate the different behaviours of the calculated values for f and β over time a comparison of the methods within the stable periods is shown in Fig. 8.

6.4. Generalisation

To extend our investigations beyond only the wheat plants we have used thus far, we also evaluate data from three commonly available plant types exhibiting various oscillatory behaviours. Specifically, we analyse the behaviour of a hanging vine of *Epipremnum aureum* ("golden pothos", Scenario 6, see Fig. 9a), the stem of a *Ficus elastica* ("rubber tree", Scenario 7, see Fig. 9b) and various branches of a *Zamioculcas zamiifolia* ("ZZ plant", Scenarios 8 - 10, see Fig. 9c, Fig. 9d & Fig. 9e) exhibiting different degrees of overhang. The GT values for f and β for these respective Scenarios are given in Table 3.

As above, we investigate the performance of HI with an increasing-size window and of FFT with an increasing-size window for f as well as with a fixed-size window for β. The results for these experiments are given in Table 4.

Figure 8: Calculation of frequency (left) and decay (right) values in the stable periods (visualised as blue background) for Scenarios 1 - 5 (top to bottom) by FFT (red) and HI (orange). All calculations were done using an increasing-size window except for the calculation of decay by FFT, for which a fixed-size window of 1.0 s was used.

Scenario		#6	#7	#8	#9	#10
HI	f	1.2 %	0.5 %	1.7 %	0.7 %	4.1 %
	β	39.5 %	17.9 %	14.3 %	8.6 %	17.0 %
FFT	f	7.8 %	6.0 %	6.7 %	4.2 %	6.5 %
	β	35.4 %	14.7 %	12.1 %	2.3 %	17.2 %

Table 4: Mean percentage error for frequency and decay of various plants calculated using HI or FFT respectively. A moving evaluation window (T = 1.0 s) was used for the calculation of β by FFT and an increasing-size window for all other calculations.

It can be seen that the approach generalises well to other scenarios, albeit with some caveats. As before, the best results for f are consistently obtained through HI with an increasing value for T. For β, HI again produces slightly

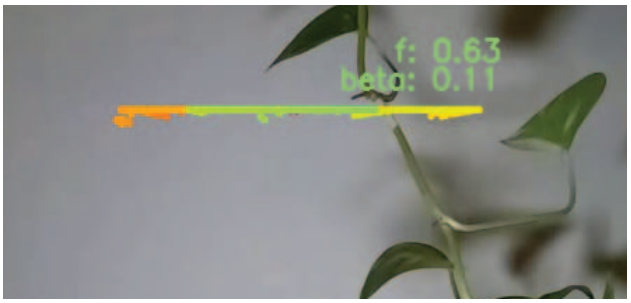

(a) *Epipremnum aureum*, Scenario 6

(b) *Ficus elastica*, Scenario 7

(c) *Zamioculcas zamiifolia*, Scenario 8

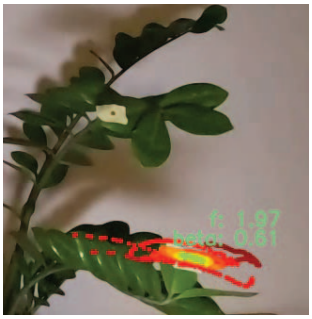

(d) *Zamioculcas zamiifolia*, Scenario 9

(e) *Zamioculcas zamiifolia*, Scenario 10

Figure 9: Different types of plants used in our experiments. The oscillatory motion the plants exhibited during the experiments are shown as a trace of the markers applied along with the respective values for f [Hz] and β [s^{-1}].

worse results than FFT, however again the differences in the mean errors are small. The worst results for decay values are achieved for Scenario 6, i.e. the hanging vine, since it exhibits very low damping (see Table 3). It is therefore hard for the algorithm to detect any noticeable decay in the time frame of the investigation. This behaviour could theoretically be improved by extending the data collection period significantly, but due to the low magnitude of β, very low noise values still have a comparatively large impact on the relative mean error.

Overall, however, HI performs significantly better in terms of frequency estimates in all scenarios and similarly as good as FFT for obtaining decay values. Additionaly, as highlighted previously, FFT based methods require additional computation steps to get a measure of the decay values while HI does not.

7. Conclusions

In this paper, we have presented a method for automated estimation of the short-term dynamic oscillatory parameters of plants which hold the potential for significantly improving the process of high-throughput phenotyping. We have employed modern computer vision techniques aided by harmonic inversion to obtain estimates for these parameters from standard video sequences and compared the results to those obtained with Fourier transform based methods, which were used as a baseline. We have evaluated both methods in various configurations, different data acquisition scenarios, varying size of the sampling windows used and on different types of plants under investigation. The experiments have shown that HI provides significantly better frequency estimates than DFT and decay values that are similar to those obtained by progressively collecting signal amplitudes with DFT and fitting an exponential decay curve to those. Due to this increased complexity of DFT based methods, HI is more suitable for this task as it can be used directly without any secondary computation steps.

Obtaining these dynamic plant parameters reliably can bring huge benefits to modern agricultural tasks such as high-throughput phenotyping, as highlighted by a lot of the recent research given in Section 2. It also makes it possible to monitor plant state, identify plant parts of similar oscillatory behaviour and improve other tasks with high automation potential, which is crucial to accommodate the needs of modern agriculture.

In order to obtain robust results, HI requires a relatively narrow frequency range of interest as described in Section 5.1, which limits its applicability without any prior knowledge of the system. In future work, we will investigate a combined approach of DFT and HI, pursuing a coarse-to-fine approach, where an initial result for f is provided through DFT which is subsequently refined with the help of HI while simultaneously producing accurate values for β. Furthermore we have not addressed the issue of automated tracking of plant parts in this paper, as previous work investigates this problem and we focus mostly on the processing of these data. A complete system however would need to incorporate both components, data acquisition and processing. Future work could possibly also utilise the phase information ϕ intrinsically provided by both HI and DFT to further improve the results from the analyses.

References

[1] Alex Bewley, Zongyuan Ge, Lionel Ott, Fabio Ramos, and Ben Upcroft. Simple online and realtime tracking. In *2016 IEEE International Conference on Image Processing (ICIP)*, pages 3464–3468, 2016. 3

[2] Yashraj Bhosale, Ehsan Esmaili, Kinjal Bhar, and Sunghwan Jung. Bending, twisting and flapping leaf upon raindrop impact. *Bioinspiration & Biomimetics*, 15, 01 2020. 2

[3] Franka Brüchert, Olga Speck, and Hanns-Christof Spatz. Oscillations of plants' stems and their damping: Theory and experimentation. *Philosophical transactions of the Royal Society of London. Series B, Biological sciences*, 358:1487–92, 10 2003. 2

[4] Sergio Castro-Garcia, Gregorio Blanco-Roldán, Jesús Gil-Ribes, and Juan Agüera Vega. Dynamic analysis of olive trees in intensive orchards under forced vibration. *Trees - Structure and Function*, 22:795–802, 12 2008. 2

[5] Emmanuel de Langre. Plant vibrations at all scales: a review. *Journal of Experimental Botany*, 70(14):3521–3531, 05 2019. 2

[6] Emmanuel de Langre, Olivier Penalver, Pascal Hémon, Jean-Marie Frachisse, Marie-Béatrice Bogeat-Triboulot, Benjamin Niez, Éric Badel, and Bruno Moulia. Nondestructive and fast vibration phenotyping of plants. *Plant Phenomics*, 2019, 2019. 2

[7] Charles R. Harris, K. Jarrod Millman, Stéfan J. van der Walt, Ralf Gommers, Pauli Virtanen, David Cournapeau, Eric Wieser, Julian Taylor, Sebastian Berg, Nathaniel J. Smith, Robert Kern, Matti Picus, Stephan Hoyer, Marten H. van Kerkwijk, Matthew Brett, Allan Haldane, Jaime Fernández del Río, Mark Wiebe, Pearu Peterson, Pierre Gérard-Marchant, Kevin Sheppard, Tyler Reddy, Warren Weckesser, Hameer Abbasi, Christoph Gohlke, and Travis E. Oliphant. Array programming with NumPy. *Nature*, 585(7825):357–362, Sept. 2020. 4

[8] Ola Heide, J Stavang, and Anita Sønsteby. Physiology and genetics of flowering in cultivated and wild strawberries - a review. *Journal of Horticultural Science and Biotechnology*, 88, 01 2013. 2

[9] Ken James, N. Haritos, and Peter Ades. Mechanical stability of trees under dynamic loads. *American journal of botany*, 93:1522–30, 10 2006. 2

[10] Katherine James, Daniel Sargent, Adam Whitehouse, and Grzegorz Cielniak. High-throughput phenotyping for breeding targets—current status and future directions of strawberry trait automation. *Plants, People, Planet*, 4, 06 2022. 1, 2

[11] Stephen G. Johnson. harminv. `https://github.com/NanoComp/harminv`, 2023. 4

[12] M. J. Jonsson, Andrea Foetzki, Markus Kalberer, Tor Lundström, Walter J. Ammann, and Veronika Stöckli. Natural frequencies and damping ratios of norway spruce (picea abies (l.) karst) growing on subalpine forested slopes. *Trees*, 21:541–548, 2007. 2

[13] Sunghwan Jung, Jisoo Yuk, and Matthieu Fuchs. Measuring fluttering frequency of a leaf under water stress. *Authorea Preprints*, 11 2021. 2

[14] Federico Magistri, Nived Chebrolu, and Cyrill Stachniss. Segmentation-based 4d registration of plants point clouds for phenotyping. In *2020 IEEE/RSJ International Conference on Intelligent Robots and Systems (IROS)*, pages 2433–2439, 2020. 2

[15] J Main, P A Dando, Dz Belkic, and H S Taylor. Decimation and harmonic inversion of periodic orbit signals. *Journal of Physics A: Mathematical and General*, 33(6):1247–1263, feb 2000. 4

[16] Jörg Main, Vladimir A Mandelshtam, Günter Wunner, and Howard S Taylor. Harmonic inversion as a general method for periodic orbit quantization. *Nonlinearity*, 11:1015 – 1035, 1998. 4

[17] Vladimir A Mandelshtam. On harmonic inversion of cross-correlation functions by the filter diagonalization method. *Journal of Theoretical and Computational Chemistry*, 02:497–505, 2003. 4

[18] Vladimir A. Mandelshtam and Howard S. Taylor. Harmonic inversion of time signals and its applications. *The Journal of Chemical Physics*, 107(17):6756–6769, 1997. 3, 4

[19] Megan Mathey, Sonali Mookerjee, Kazim Gunduz, James Hancock, Amy Iezzoni, Lise Mahoney, Thomas Davis, Nahla Bassil, Kim Hummer, Philip Stewart, Vance Whitaker, Daniel Sargent, Béatrice Denoyes, Iraida Amaya, Eric Van de Weg, and Chad Finn. Large-scale standardized phenotyping of strawberry in rosbreed. *Journal- American Pomological Society*, 67:205–216, 10 2013. 2

[20] Miyuki Nakata, Masahiro Takahara, Shingo Sakamoto, Kouki Yoshida, and Nobutaka Mitsuda. High-throughput analysis of arabidopsis stem vibrations to identify mutants with altered mechanical properties. *Frontiers in Plant Science*, 9, 06 2018. 2

[21] C.E. Shannon. Communication in the presence of noise. *Proceedings of the IRE*, 37(1):10–21, jan 1949. 4

[22] Hanns-Christof Spatz, Franka Brüchert, and Jochen Pfisterer. Multiple resonance damping or how do trees escape dangerously large oscillations? *American journal of botany*, 94:1603–11, 10 2007. 1, 2

[23] Hanns-Christof Spatz and Benoit Theckes. Oscillation damping in trees. *Plant Science*, 207:66–71, 2013. 2

[24] Petre Stoica, Randolph L Moses, et al. *Spectral analysis of signals*, volume 452. Pearson Prentice Hall Upper Saddle River, NJ, 2005. 3

[25] Loïc Tadrist, Marc Saudreau, Pascal Hémon, Xavier Amandolese, André Marquier, Tristan Leclercq, and Emmanuel de Langre. Foliage motion under wind, from leaf flutter to branch buffeting. *Journal of The Royal Society Interface*, 15:20180010, 05 2018. 2

[26] Nikolaus Wagner and Grzegorz Cielniak. Inference of mechanical properties of dynamic objects through active perception. In Charles Fox, Junfeng Gao, Amir Ghalamzan Esfahani, Mini Saaj, Marc Hanheide, and Simon Parsons, editors, *Towards Autonomous Robotic Systems*, pages 430–439, Cham, 2021. Springer International Publishing. 2, 3

[27] Ya Xiong, Yuanyue Ge, and Pål Johan From. An improved obstacle separation method using deep learning for object detection and tracking in a hybrid visual control loop for fruit

picking in clusters. *Computers and Electronics in Agriculture*, 191:106508, 2021. 1

[28] Wanneng Yang, Hui Feng, Xuehai Zhang, Jian Zhang, John H. Doonan, William David Batchelor, Lizhong Xiong, and Jianbing Yan. Crop phenomics and high-throughput phenotyping: Past decades, current challenges, and future perspectives. *Molecular Plant*, 13(2):187–214, 2020. 1